2012 NDIA GROUND VEHICLE SYSTEMS ENGINEERING AND TECHNOLOGY SYMPOSIUM
MODELING & SIMULATION, TESTING AND VALIDATION (MSTV) MINI-SYMPOSIUM
AUGUST 14-16, MICHIGAN

INVESTIGATION OF STRESS AND FAILURE IN GRANULAR SOILS FOR LIGHTWEIGHT ROBOTIC VEHICLE APPLICATIONS

Carmine Senatore
Massachusetts Institute of Technology
Cambridge, MA, USA

Markus Wulfmeier
Gottfried Wilhelm Leibniz Universität Hannover
Hannover, Germany

Jamie MacLennan
Paramsothy Jayakumar
U.S. Army TARDEC
Warren, MI, USA

Karl Iagnemma
Massachusetts Institute of Technology
Cambridge, MA, USA

ABSTRACT

This paper describes novel experimental methods aimed at understanding the fundamental phenomena governing the motion of lightweight vehicles on dry, granular soils. A single-wheel test rig is used to empirically investigate wheel motion under controlled wheel slip and loading conditions on sandy, dry soil. Test conditions can be designed to replicate typical field scenarios for lightweight robots, while key operational parameters such as drawbar force, torque, and sinkage are measured. This test rig enables imposition of velocities, or application of loads, to interchangeable running gears within a confined soil bin of dimensions 1.5 m long, 0.7 m wide, and 0.4 m deep. This allows testing of small-scale wheels, tracks, and cone or plate penetrators. Aside from standard wheel experiments (i.e., measurements of drawbar force, applied torque, and sinkage during controlled slip runs) two additional experimental methodologies have been developed. The first relies on high-speed imaging of the wheel-soil interface and the use of particle image velocimetry (PIV) to measure micro-scale terrain kinematics. The second experimental methodology consists of a custom force sensor array located at the wheel-terrain interface. The sensors allow explicit measurement of normal and shear forces (and, therefore, estimation of normal and shear stresses) at numerous discrete points along the wheel-soil interface. Experimental measurements gathered by these test methodologies are to be compared against well-established semi-empirical models, to validate and understand limitations of the models and propose improvements.

INTRODUCTION

Robotic vehicles are frequently deployed in unwelcoming, hazardous environments. From military robots to planetary rovers, vehicle mobility is a key aspect of mission success. Several models for traction modeling of tracked and wheeled vehicles have been developed in the past decades; however, a comprehensive understanding of soil behavior under running gear is still missing to date. The work of Bekker and Wong, which began in the 1950's, has laid the foundation for modern terramechanics. The application of classical results from plasticity theory, combined with semi-empirical formulations, has provided satisfactory solutions to the problem of mobility modeling for large, heavy vehicles. However, the expanded use of lightweight vehicles (especially man-portable robotic vehicles) has called for a new effort in modeling vehicle-terrain interaction problems. In fact, some researchers have suggested that classical models are of questionable utility when applied to vehicles one order (or more) of magnitude smaller than tanks, Humvees, large trucks, and the like [1].

This paper will describe novel experimental methods aimed at understanding the fundamental phenomena governing the motion of lightweight vehicles on dry, granular soils. A single-wheel test rig is used to empirically investigate wheel motion under controlled wheel slip and loading conditions on a sandy, dry soil (Figure 1). Test conditions can be designed to replicate typical field scenarios for lightweight robots, while key operational parameters such as drawbar force, torque, and sinkage are

measured. This test rig enables imposition of velocities, or application of loads, to interchangeable running gears within a confined soil bin of dimensions 1.5 m long, 0.7 m wide, and 0.4 m deep. This allows testing of small-scale wheels, tracks, and cone or plate penetrators.

The soil under investigation has been fully characterized with a series of direct shear tests (ASTM D3080) and penetration tests. Direct shear tests were performed to estimate soil shearing parameters such as cohesion, angle of internal friction, and shear modulus. Penetration tests, although not standard tests, were performed to evaluate 'Bekker' parameters, necessary for characterization of pressure-sinkage behavior of the soil under the methodology described by Wong [2].

The aforementioned experiments represent a typical experimental approach to macro-scale characterization of wheel-soil interaction. However, the application of classical terramechanics model to lightweight vehicles may potentially show discrepancy between experiments and predictions, warranting the development of new methods to probe the fundamental mechanics of a small robot's interaction with soil.

To this end, two additional experimental methodologies have been developed. The first relies on high-speed imaging of the wheel-soil interface and the use of particle image velocimetry (PIV) to measure micro-scale terrain displacement (Figure 1). This methodology, although confined to plane strain cases, allows measurement of soil flow velocities, and observation of the formation of shear bands beneath the wheel/track. Though this method does not explicitly permit calculation of the velocities of individual soil particles, it does allow estimation of a regularly-spaced velocity field in the soil. While such visualization techniques have been widely employed in the field of experimental fluid mechanics, their application to the study of soils is a relatively new development [3, 4].

The second experimental methodology is intended to complement the PIV-based soil kinematics analysis. It employs a custom force sensor array located at the wheel-terrain interface. The force sensors are strain gauge-based flexural elements with interchangeable interface surfaces that are designed for integration with wheels or other running gear. The sensors allow explicit measurement of normal and shear forces (and, therefore, estimation of normal and shear stresses) at numerous discrete points along the wheel-soil interface. When coupled with PIV-derived kinematic data, this allows for a richer characterization of soil loading and failure regimes than would be possible with either kinematic or pressure information alone. In particular, this experimental methodology allows joint visualization of the soil displacement in the bulk soil medium, and measurement of shear and normal stress at points along the interface. This could lead to development and validation of novel constitutive relations describing soil behavior under loading imposed by running gear.

Experiments have shown that soil failure, at certain slip levels, is qualitatively different under cases of low vertical load (which is typical for lightweight robots) compared to cases of high vertical load (typical for large ground vehicles). Also, soil flow patterns have been observed to exhibit periodic failure phenomena, giving rise to interesting features such as surface ripple formation. These results, obtained through PIV analysis, provide deeper understanding of the mechanics of traction generation. Experimental measurements gathered by these test methodologies are compared against the results from well-established semi-empirical models, to understand limitations of these models and propose modifications and improvements.

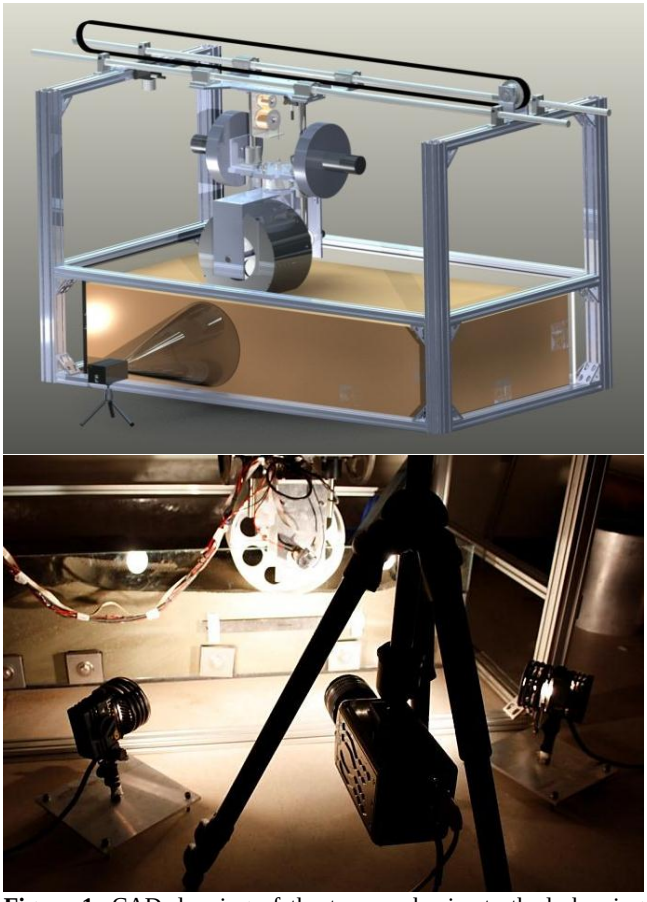

Figure 1: CAD drawing of the terramechanics testbed showing the imager for PIV experiments (top). Actual PIV setup with the high speed camera and two flood lights (bottom).

SINGLE WHEEL TESTBED DESCRIPTION

The Robotic Mobility Group at MIT has designed and fabricated a multipurpose terramechanics rig based on the standard design described by Iagnemma [5]. The testbed is pictured in Figure 1 and is composed of a Lexan soil bin surrounded by an aluminum frame where all the moving parts, actuators and sensors are attached. A carriage slides on two low-friction rails to allow longitudinal translation while the wheel or track, attached to the carriage, is able to rotate at a desired angular velocity. The wheel mount is also able to translate in the vertical direction. This typical setup allows control of slip and vertical load by modifying the translational velocity of the carriage, angular velocity of the wheel, and applied load. Horizontal carriage displacement is controlled through a toothed belt, actuated by a 90W Maxon DC motor while the wheel is directly driven by another Maxon DC motor. The motors are controlled thorough two identical Maxon ADS 50/10 4-Q-Dc servoamplifiers. The carriage horizontal displacement is monitored with a Micro Epsilon WPS-1250-MK46 draw wire encoder while wheel vertical displacement (i.e., sinkage) is measured with a Turck A50 draw wire encoder. A 6-axis force torque ATI Omega 85 transducer is mounted between the wheel mount and the carriage in order to measure vertical load and traction generated by the wheel. Finally, a flange-to-flange reaction torque sensor from Futek (TFF500) is used to measure driving torque applied to the wheel. Control and measurement signals are handled by a NI PCIe-6363 card through Labview software.

The rig is capable of approximately 1 meter of horizontal displacement at a maximum velocity of approximately 120 mm/s with a maximal wheel angular velocity of approximately 40 deg/s. The bin width is 0.6 meters while the soil depth is 0.16 meters. Considering the wheel sizes and vertical loads under study, these physical dimensions are sufficient for eliminating boundary effects. Moreover, the same testbed, with some adaptations, can be used to perform soil penetration tests and analyze different running gears (e.g., both wheels and tracks).

For the experiments described in this paper, the Mojave Martian Simulant (MMS) was employed as a test medium [6]. MMS is a mixture of finely crushed and sorted granular basalt intended to mimic, both at chemical and mechanical level, Mars soil characteristics. MMS particle size distribution spans from micron level to mm level with 80% of particles above the 10 micron threshold.

GRANULAR SOIL PARTICLE IMAGE VELOCIMETRY

Particle image velocimetry (PIV) describes an experimental method, based on image cross-correlation techniques, used for the determination of flow velocity fields. The use of PIV for the calculation of fluid velocities initially emerged in the 1980‘s [7, 8]. Since then, PIV has played an important role in many fluid mechanics investigations [9]. Two of the main advantages of PIV over other methods for the measurement of velocity (e.g. hot-wire-velocimetry, Pitot tubes etc.) are that it is non-intrusive, and allows for relatively high resolution measurements over an extended spatial domain.

During fluid-based PIV analysis, the fluid is typically seeded with marker particles that refract, absorb, or scatter light, have a high contrast with the fluid, and do not interrupt the fluid flow. Imaging is performed at high speed over an area of the flow illuminated by a light source, typically a pulsed laser. Captured images are post-processed with algorithms that perform frame-to-frame feature tracking and calculation of flow velocity fields.

PIV is also a useful method for measuring soil motion, with the notable constraint that soil is typically observed through a glass sheet, limiting the resulting analysis to plane strain scenarios. The natural granular texture of soils often generates an intensity pattern that can be readily traced by PIV-algorithms, without the use of marker particles. Also, incandescent light can generally be used for illumination.

Granular PIV has recently been employed in several applications, including the analysis of grains in converging hoppers [10], study of flowing granular layers in rotating tumblers [11], investigation of granular avalanches [12], analysis of soil motion caused by the movement of animals [13], the study of burrowing behavior of razor clams [3], and in the study of wheel-soil interaction [4, 14]. The analysis of soil motion beneath a driven wheel via quantitative analysis of successive temporal images was first introduced by Wong [15]. However, the experimental capabilities of that study did not allow for high-speed image capture, limiting the accuracy and practical utility of the method.

Soil motion analysis can be broken down into four main steps: 1) image acquisition, 2) image pre-processing, 3) image cross-correlation (PIV), and 4) velocity field post-processing. These steps are briefly described here, and methods for parameter selection are presented. Note that in the following, the Matlab-based PIVlab software is employed [16].

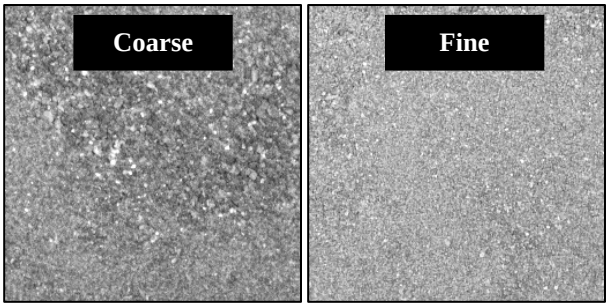

Figure 2: Examples of soil natural textures.

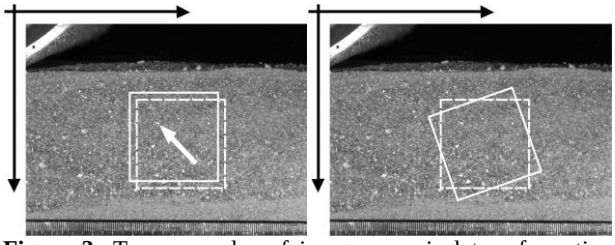

Figure 3: Two examples of image canonical transformations used to evaluate PIV settings. Nine image transformations for coarse and fine soil textures were used to evaluate PIV accuracy.

PIV IMAGER CONFIGURATION

The accuracy of PIV strongly depends on the quality of the captured images. For these experiments the testbed was fitted with a 2.54 cm thick tempered glass wall while the running gear was operated flush against this surface (see Figure 1). Both wheels and tracks have been analyzed with this testbed, however this paper describes results from rigid wheel testing.

Image sets for the PIV measurement were captured with a Phantom 7 high-speed camera. The Phantom 7 is able to record grayscale images at the maximum resolution of 800x600 pixels at a maximum frame rate of 6688 fps. The camera was placed perpendicular to the front glass wall (see Figure 1) at a distance of 52 cm, while the focal length was set to 77 mm (a zoom lens was used) resulting in an image capture region of approximately 15 x 11.25 cm. It should be noted that determination of image capture region size is largely dictated by the particular experimental conditions. Here, the image capture region was chosen in order to conservatively bound the region of soil that would undergo motion when subjected to wheel passage on the soil surface. Two 250W Lowel Pro-Light photography flood lights were placed on either side of the camera at an angle of 45° towards the object plane, and provided approximately homogeneous illumination of the soil. By using two laterally positioned light sources, reflections and shadows can be significantly diminished.

PIV IMAGE PREPROCESSING

The performance of PIV cross-correlation algorithms generally improves when images are of high contrast, feature dense, and have low noise. In practice, images are subject to nonuniform illumination, image sensor noise, and lack of natural contrast in the granular material, all of which can degrade PIV algorithm performance. Various image pre-processing methods were investigated to understand their effect on algorithm performance. These include commonly-employed algorithms such as contrast limited adaptive histogram equalization, high pass filtering, and clipping and intensity capping.

To systematically investigate the effect of these preprocessing methods on PIV algorithm performance, test image segments of the Mars regolith simulant with dimensions 256 x 256 pixels were captured, then synthetically deformed in canonical directions. Since the particle distribution in the soil under investigation is locally inhomogeneous, two distinct image segments were captured in order to adequately represent typical apparent grain distributions in the MMS simulant. This resulted in one image populated by relatively large grains and one populated by relatively small grains (Figure 2). Synthetic deformation of the image was performed as a means of generating a ground truth for cases of linear translation (1-4 pixels in both horizontal, vertical, and diagonal directions), rotation (1-8 degrees in clockwise and counter-clockwise directions), shear (1-4 pixels of relative motion between upper and lower image halves), and simple shear (1-4 pixels of motion of upper edge of image) (Figure 3). Since the pixel shift for each deformation was controlled, this methodology allowed quantitative evaluation of PIV algorithm results. An error metric was computed by computing the average difference, over all points in the PIV velocity field, between the velocity vector calculated through PIV and the true velocity vectors.

PIV IMAGE CROSS-CORRELATION

In PIV, images are divided into small interrogation windows (IW) and then analyzed to compute the probable displacement between successive images for each IW using cross-correlation techniques. This results in an equally spaced field of calculated velocity vectors. The probable displacement is determined by using the cross-correlation function:

$$R_{II'}(x,y) = \sum_{i=-K}^{K} \sum_{j=-L}^{L} I(i,j)\, I'(i+x, j+y) \qquad (1)$$

where I is the intensity of the first image and I' the intensity of the second image. A detailed description of PIV theory can be found in [17]. Particle density, image resolution, and IW size are interconnected parameters that must be carefully selected to optimize performance. Based on experimental investigations, Keane and Adrian [18] defined empirical

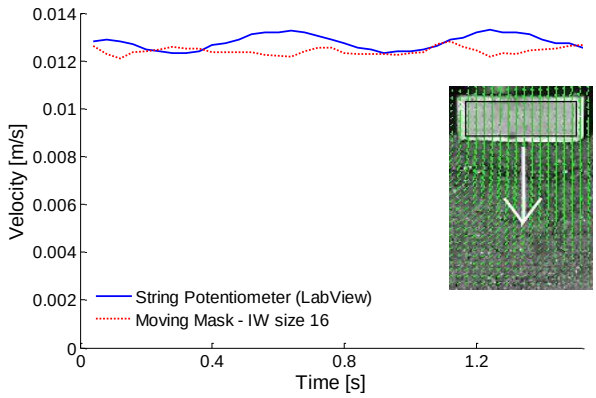

Figure 4: Comparison of velocity calculated through PIV and measured with a draw wire encoder.

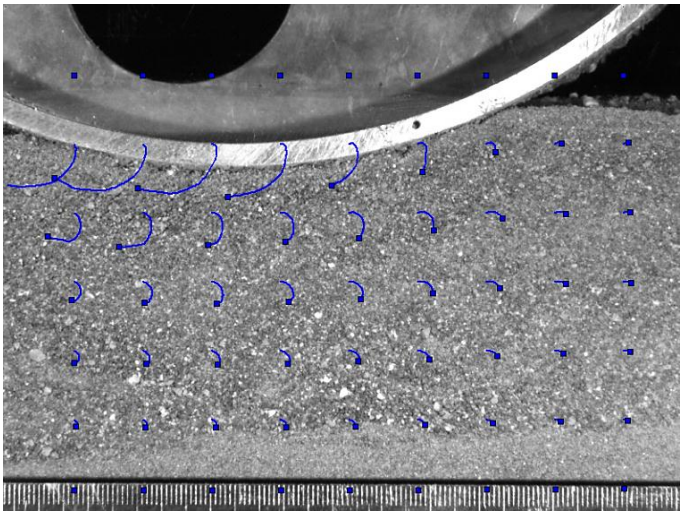

Figure 5: Soil trajectories calculated from velocity field obtained through PIV analysis. Visual inspection showed that PIV yielded tracking of soil regions on the order of 0.5-1 mm after translations of several centimeters.

rules for optimal PIV setup. The reader is referred to the above paper for more details. For the results presented here, the following settings were employed: 25 fps, final IW size of 16, CLAHE filtering with kernel size of 40 pixels. A more complete description of the PIV settings and analysis is presented in [19].

VELOCITY FIELD POST-PROCESSING

The raw velocity field produced by PIV calculations can contain spurious vectors (outliers). These outliers can be caused by noise, inappropriate interrogation settings, and accidentally matched patterns. Hence, to improve results, rejection of these outliers and interpolation of missing data points can be performed in a post-processing stage through filtering. Filters for the rejection of outliers can primarily be divided into two separate classes: global and local methods. Global filters commonly employ a simple thresholding method, with the threshold value selected by an operator with empirical or theoretical domain knowledge. If elements of the velocity field exceed the threshold, this element is removed from the results. Local filters are primarily based on relative differences between surrounding vectors, rather than absolute values. A local filter calculates the mean and standard deviation of the velocity for a selected kernel size around each vector. If the velocity exceeds certain thresholds, the vector is rejected. For the results presented here, a 5x5 kernel with a threshold of 8 times the standard deviation was used for post-processing.

VALIDATION AND VERIFICATION

The synthetically deformed image was determined to be a useful ground truth for determining appropriate PIV operational parameters. However, validation of the PIV algorithm performance was also pursued on two sets of test data that were physically relevant to the running gear-soil interaction case.

The first test consisted of calculating the velocity via PIV of a 2.5 cm thick steel plate performing a soil penetration test. The ground truth velocity of the plate was externally measured by numerically differentiating the output of the draw wire encoder (which nominally provides a position measurement). To obtain a plate velocity measure from PIV, an average of the velocities was computed over a rectangular region of interest aligned with the moving plate.

Figure 4 shows a comparison of the plate velocity as determined from PIV calculations and the velocity measured by the draw wire encoder. The average percent error (for the best settings) between these measurements was below 1%. It should be noted that, for this test case, the PIV algorithm is not performing calculations on the granular soil, but rather the steel plate edge. However, this test remains of interest since the soil in contact with the plate necessarily moves at the same velocity.

The second test consisted of calculating the time evolution of motions of discrete features associated with MMS simulant soil beneath a driven rigid wheel. Trajectories $s(t)$ are calculated for a grid of 9 x 6 regions of interest over the soil area. The time evolution of the positions of the center of the regions of interest was computed by integrating the velocities with a fourth order Runge-Kutta method.

$$s(t) = \int_0^t v(t)dt \qquad (2)$$

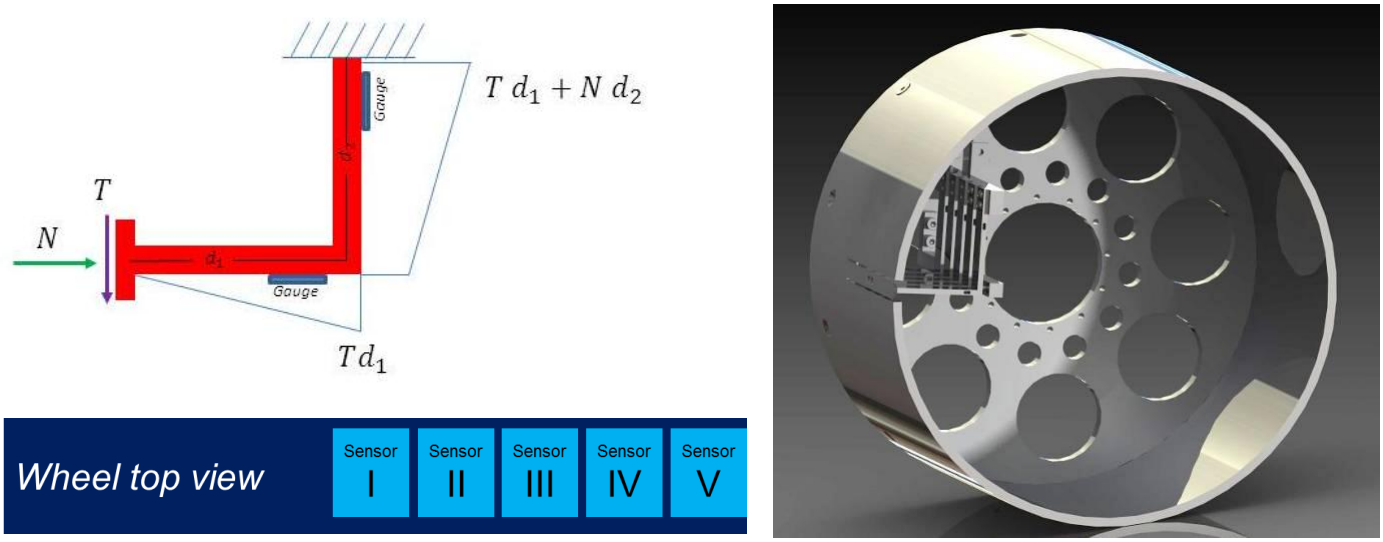

Figure 6: Working scheme of the custom force sensor for interfacial stress measurement (top left). Five sensors are distributed from the wheel median axis to the wheel edge (bottom left). Sensors are rigidly connected to the wheel hub (right)

The motion of these tracked regions were compared to trajectories of individual soil particles that are large enough to be manually tracked from frame to frame, thereby providing a qualitative performance evaluation. Also, the calculation of feature trajectories is useful for illustrating soil flow when subjected to various loading conditions.

Figure 5 displays the trajectories computed while the wheel was advancing at 17 deg/s with 30% slip. Note that the area above the soil surface was masked during pre-processing, and hence these features remain at their original location. The squares show the final position of the tracked features and the lines represent the motion evolution. Manual inspection showed that the selected PIV yielded tracking of soil regions in the order of 1-2 pixels, corresponding to 0.5-1 mm after translations of several centimeters.

WHEEL-TERRAIN INTERFACE FORCE SENSOR DESCRIPTION

Measurement of the normal and shear stress acting on a moving wheel is important for empirical testing and validation of models describing interfacial phenomena. While numerous COTS sensors exist for measuring pressure [20], the authors are unaware of any available sensors that can measure both pressure and shear stress, at a scale and resolution suitable for investigation of the interaction mechanics of small, lightweight vehicle running gear and deformable soil.

Therefore, a custom sensor array was designed and fabricated (Figure 6). Each sensor is a solid-state L-shaped aluminum flexure instrumented with two full bridge strain gages. The sensor is mounted rigidly to the running gear, and its interface element is exposed to the soil. The interface element is generally subjected to normal (N) and shear (T) loading. These forces cause the flexure elements to deflect in a linear elastic manner. From measured deflection, and given prior calibration data, the applied forces can be uniquely computed. (Axial strain is intrinsically rejected by the full bridge configuration.) Stress can then be inferred assuming uniform pressure distribution over the known sensors' head area.

Sensors are mounted on the surface of a 26 cm diameter rigid aluminum wheel (see Figure 6). Note that a twin wheel, without the array, was used for PIV testing. Five sensors have been fabricated and integrated in a linear array spanning one half of the wheel width (i.e. from one edge to the center of the wheel). Sensors were first calibrated by applying test weights of 100, 200, and 500 grams in the normal and tangential direction. Measurement linearity error, across all the sensors, was found to be below 3%.

The sensor array is extremely sensitive to misalignment and thus an uneven contact patch profile can easily unbalance the output reading. To ensure accurate alignment, sensors alignment was verified after every 5 tests, by driving the wheel over a flat, rigid, aluminum plate covered with a thin layer of polyurethane foam in order to verify that the sensor output was uniform. Due to the difficulty in precisely controlling soil preparation, each test was repeated at least 15 times. In fact, local soil density variation, inhomogeneity (due to non-uniform distribution of larger grains, for example), and surface unevenness all were observed to affect measurement output. The 15 trials highlighted test

variability and were analyzed to detect outliers and eventually remove tests where anomalies were detected.

SOIL PROPERTIES

Characterization of the soil under investigation is a necessary step for any terramechanics investigation. Detailed chemical composition, particle size distribution, and shearing properties of the MMS simulant under investigation can be found in [6]. However, pressure-sinkage properties (i.e. Bekker's parameters) for the soil were unknown, and therefore a series of plate penetration tests were performed.

Since the wheel has a width of 0.13 m and a nominal contact patch length of 0.05 m (estimated assuming nominal conditions of Fz = 100 N and low slip) three rectangular plates with the following dimensions were selected: 0.13 m x 0.03 m, 0.13 m x 0.05 m, and 0.13 m x 0.07 m.

Each plate was mounted on a linear actuator, which was anchored to the testbed and then pushed perpendicularly into the soil while the vertical load and penetration length (i.e. sinkage) were measured with a load cell and a draw wire encoder, respectively.

For each plate, tests were repeated 15 times. Between each test, soil was manually agitated and then re-leveled. Figure 7 shows an example of the data collected. Test-to-test variation was observed, but was not considered unusual due to the nondeterministic nature of soil testing.

The scope of the tests was to fit experimental data to Bekker's pressure-sinkage equation [21]:

$$p = \left(\frac{k_c}{b} + k_\phi\right) z^n \tag{3}$$

where p is pressure, z is sinkage, b is plate width (3,5,7 cm) and $\{k_c, k_{phi}, n\}$ are the parameters under investigation. Adopting the fitting methodology presented in [2] it was noted that $k_{eq_b} = \left(\frac{k_c}{b} + k_\phi\right)$ is strongly correlated with n as shown in Figure 8. This correlation necessarily results from the tests having similar amounts of deviation from an exponential curve. While this effect is solely an artifact of experimental estimation, it is still undesirable because it inhibits k_{eqb} from being estimated independently.

The problem is mitigated through adoption of Reece's equation [22] for pressure-sinkage:

$$p = k_{eq_r} \left(\frac{z}{b}\right)^n \tag{4}$$

Dimensional analysis of Reece's equation shows that k_{eq_r} is not function of n (as it was in Bekker equation). Although variability is still substantial, k_{eq_r} estimation becomes less dependent of n as can be seen in Figure 9.

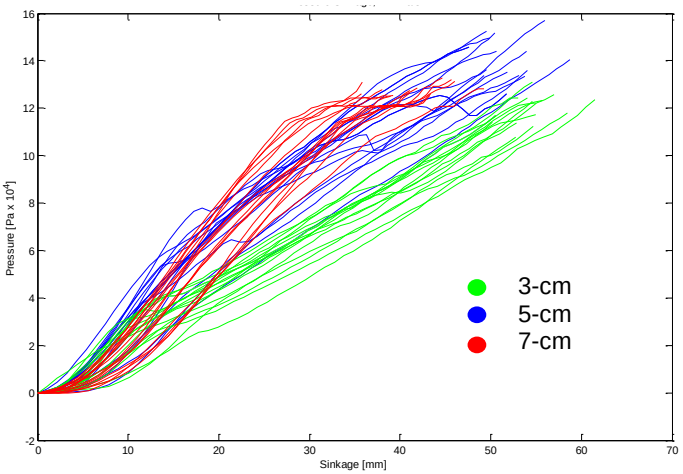

Figure 7: Penetration tests for rectangular plates with the following dimensions 0.13 m x 0.03 m, 0.13 m x 0.05 m, 0.013 x 0.07 m.

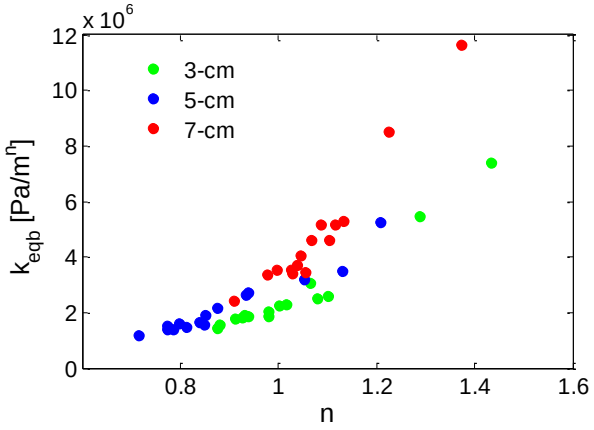

Figure 8: Strong correlation between soil parameters when Bekker equation is used.

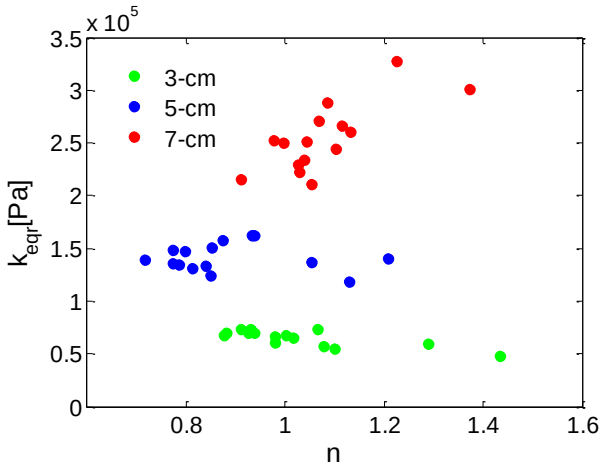

Figure 9: Correlation between soil parameters is mitigated when Reece's equation is used.

Penetration tests variability, even under laboratory controlled conditions, suggests that soil parameters should be derived from statistical distributions rather than deterministic values. A stochastic characterization of terrain properties is currently being investigated by the authors while the results presented in this paper are still derived with the method established by Wong [2].

Two parameter sets are reported in Table 1. The set labeled '357' has been obtained considering the full dataset presented in Figure 7 while the set labeled "57" has been obtained only with the 5 cm and 7 cm plates, and truncating the data at 50 kPa. This was motivated by the fact that the wheel under investigation was expected to have contact patch length larger than 5 cm and normal stress distribution below 50kPa. The two datasets show how slightly modifying the design of experiments, can drastically change soil parameter calculation.

Table 1: Bekker soil parameters for the MMS soil. Two sets were extracted, 357 includes all the data while for 57 only two plates were used (5 cm and 7 cm) and data was truncated at 50 kPa mark.

Set	n	k_c [kN/m^{n+1}]	k_ϕ [kN/m^{n+2}]
357	0.99	-55	4584
57	1.4	846	6708

RESULTS AND DISCUSSION

Experiments with the PIV and stress sensor experimental methodologies were conducted separately. For PIV tests, a smooth wheel, coated with MMS simulant (to ensure sufficient interfacial friction) was run flush against a glass wall. For stress sensor tests, a wheel of exactly the same diameter, and again covered with MMS simulant, was run in the middle of the soil bin. Soil was loosened, mixed, and leveled between each test, in an attempt to achieve uniformly loose, homogenous conditions.

Both type of tests were run at approximately 100N of vertical load and for slip levels ranging from -70% to 70% (for PIV tests, slip was limited to ±30%). For PIV tests the wheel velocity was fixed at 17 deg/s while for stress sensor tests angular velocity was reduced to 8.5 deg/s to improve measurement quality. (The horizontal carriage velocity was modified to achieve the desired slip level.) For both types of tests, it was first ascertained that velocity did not have an influence on wheel performance. The operational conditions described above were chosen because they are close to those of the Mars Exploration Rover, a successful lightweight robotic vehicle.

A substantial amount of data was collected and cannot be comprehensively described in this paper. Instead, a small number of initial results are presented.

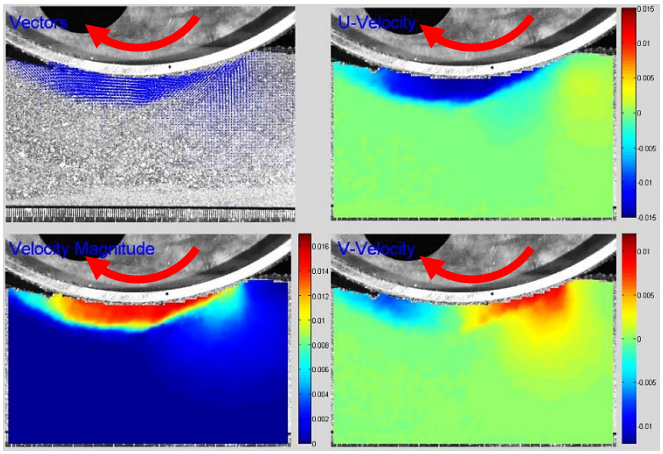

Figure 10: A snapshot of a 30% slip test. Nominal vertical load was 100N and wheel angular velocity of 17 deg/s. From top-left-clockwise: velocity vectors, u-velocity, v-velocity, and velocity magnitude.

PIV Analysis

Analysis of PIV data was performed to qualitatively analyze soil motion (a quantitative analysis would have required to investigate the complex mapping between stress and displacement, this goes beyond the scope of this preliminary study). Figure 10 presents a snapshot of a 30% slip test, and displays the following information from top-left-clockwise: velocity vectors, u-velocity, v-velocity, and velocity magnitude. Analysis of such images can provide insights into the spatial distribution of soil velocity under running gear, and can vary dramatically for such cases as slip, skid, free-rolling wheels, braked wheels, etc.

Decomposition of this flow field can yield useful insight into soil shearing (which occurs primarily in the horizontal direction, see upper right image) and soil compaction phenomena (which occurs primarily in the vertical direction, see lower right image). Here, a blue region corresponds to no motion while red indicates a maximum velocity. Analysis of these images shows that soil flow remains attached to the wheel rim. Moreover, for low vertical load (such as the one utilized during experiments) it was observed that two separate slip failure lines did not evolve, as predicted by classical theory [23, 24]. This finding is interesting because according to [23], the maximum stress occurs where the soil flow separates. The absence of flow separation, however, does not prevent stress to reach a maximum (see Figure 11).

For slip levels below ±10%, the soil was not observed to develop a significant shearing plane. Another phenomenon that was clearly highlighted by PIV analysis is the periodic nature of soil failure. For slip level above 10-15%, soil often exhibits a periodic loading cycle of alternating compaction and shearing, which results in discontinuous failure of the soil mass. This has two direct consequences: oscillations in

drawbar pull readings and creation of ripples behind the wheel. Note that while these effects have been noted previously, they have been typically assigned to the effect of grousers. However, these effects are present even for smooth wheels, without grousers.

PIV data can be useful for investigation of constitutive models for granular materials, and for development of reduced order models based on soil displacement predictions. An important consideration to bear in mind when examining flow fields like the one presented in Figure 10 is that the relationship between stress and displacement is typically complex, and one must avoid the temptation to directly (i.e., proportionally) correlate velocity magnitudes with stress magnitudes.

For this reason, direct stress measurement of shear and normal forces, and inferences of associated stresses, at the wheel-terrain interface yields valuable information about the traction generation process.

Interface Force Sensor Analysis

Classical terramechanics methods rely on the estimation of the stress distribution under the wheel. The ability to directly measure such quantities allows for a one-to-one comparison of model prediction and experimental reality.

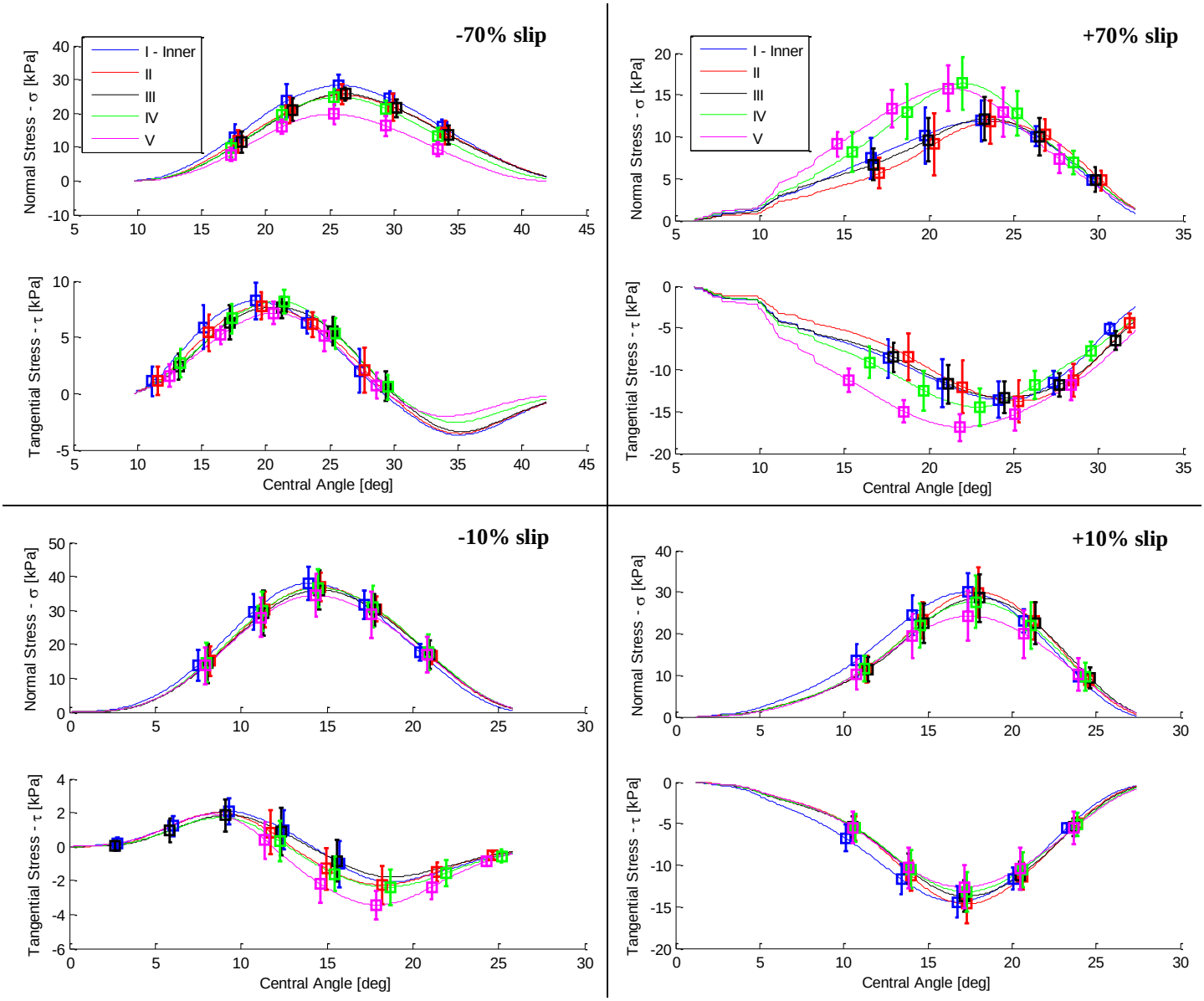

Figure 11: Normal and tangential stress at the wheel-soil interface calculated from force sensors. These were obtained for nominal vertical load of 100 N and wheel angular velocity of 8.5 deg/s. The four panels present data for -70%, +70%, -10%, and +10% slip (clockwise from upper left). Sensors are labeled according to the scheme presented in Figure 6. "I" corresponds to the sensor located at the center and "V" to the sensor located at the edge of the wheel. Central angle defines the angular position along wheel circumference [26,27].

Analysis of stress distribution across a (symmetric) half-wheel width shows that boundary effects become more pronounced as slip increases (see Figure 11). In particular, stress at the wheel edge was observed to be relatively high for positive slip and relatively low for negative slip. It is hypothesized that this effect is caused by soil transport phenomena: for positive slip, soil in the center of the wheel is transported behind the wheel at higher rate than the soil at the wheel edges, which causes the wheel edges to bear proportionally more of the total normal wheel load. On the contrary, for negative slip, soil accumulated in front of the wheel creates a thicker layer under the wheel median axis, causing higher stress in the center.

For higher loading conditions, Onafeko and Reece [25] noted that normal stress decreases with increasing positive slip since an increasingly larger portion of vertical load is supported by shear stress (which contributes more to vertical load equilibrium because of increased sinkage). This was confirmed experimentally with the stress sensors.

Another interesting aspect of wheel stress distributions is the inversion of shear stress for negative slip conditions. This phenomenon was noted also by [25] and it is consistent with wheel-soil interaction kinematics: for negative slip, the wheel travels forward but simultaneously skids over the soil, generating a shear sign transition. Interestingly, PIV imagery does not show any soil separation or flow inversion where the shear stress changes sign.

In Figure 12, a direct comparison between the measured stress and stress predicted by the model originally proposed by Wong [26, 27] and Janosi and Hanamoto [28] is presented, using the experimentally determined soil parameters (two parameter sets, presented in Table 1, are compared). The normal stress distribution is underestimated and the error seems largely related with the location of maximum stress. Tuning of semi-empirical model parameters could allow better agreement.

The predicted shear stress, however, was found to be overestimated. Note that the shear modulus adopted to produce results in Figure 12 was calculated according to [29]. For larger (but arguably inaccurate) values of shear modulus, it may be possible to obtain better agreement between prediction and experimental data; however this raises a fundamental question about the validity of the assumptions behind the model. In fact, the model assumes that the soil is sheared for a distance corresponding to the amount of relative motion between the wheel and the soil. This assumption, as shown by PIV analysis, is likely erroneous, since the soil at the wheel-terrain interface stays attached to wheel rim, while failure physically occurs (in regular, periodic failure patterns) some distance away from the interface. Although $\{n, k_c, k_\phi\}_{357}$ and $\{n, k_c, k_\phi\}_{57}$ are significantly different (see Table 1), model predictions using these two sets are relatively close. This warrants further efforts in characterizing terrain variability and its influence on stress measurements variability.

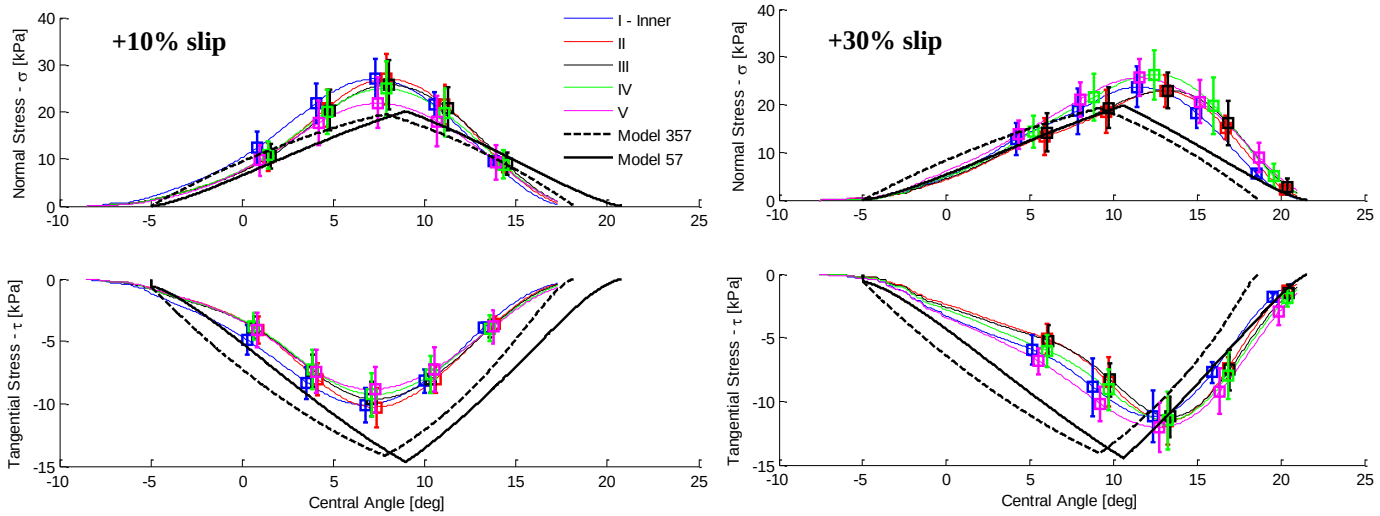

Figure 12: Stress distribution for 10% (left) and 30% (right) slip compared with analytical model from Wong and Reece [26, 27]. Two soil parameter sets, presented in Table 1, were tested. The difference between the two parameter sets, although significant, it is not dramatic. Normal stress is slightly underestimated while tangential stress is significantly estimated. Tangential stress, however, is primarily based on soil shear properties which were obtained in [29].

CONCLUSIONS

Novel experimental methods aimed at understanding the fundamental phenomena governing the motion of lightweight vehicles on dry, granular soils were presented.

Aside from standard wheel experiments (i.e., measurements of drawbar force, applied torque, and sinkage during controlled slip runs) two additional experimental methodologies were introduced. The first relies on high-speed imaging of the wheel-soil interface and the use of particle image velocimetry (PIV) to measure micro-scale terrain kinematics. The second experimental methodology consists of a custom force sensor array located at the wheel-terrain interface. The sensors allowed explicit measurement of normal and shear forces (and, therefore, estimation of normal and shear stresses) at numerous discrete points along the wheel-soil interface.

Analysis of PIV data has shown that soil failure, at certain slip levels, is qualitatively different under cases of low vertical load (which is typical for lightweight robots) compared to cases of high vertical load (typical for large ground vehicles). Also, soil flow patterns have been observed to exhibit periodic failure phenomena, giving rise to interesting features such as surface ripple formation. Soil flow was observed to be always attached to the wheel rim and only one shear failure surface was observed. Soil usually exhibits compression in front of the wheel and then shears beneath it.

Stress measurements showed that, although only one shear failure surface is present, tangential stress goes through sign inversion for negative slip. Stress distribution, along the wheel width, is approximately uniform for low slip while edge effects become increasingly significant for higher slip levels. Although some observations regarding soil shear failure were not confirmed by PIV, classical methods (partially based on those observations) were able to capture main trends for a range of slip conditions. These results provide deeper understanding of the mechanics of traction generation and are expected to open new frontiers for more accurate, and predictive, lightweight vehicle mobility models.

Further investigation of small robot-terrain interaction mechanics will focus on extending these experiments to a wider range of vertical loads. This will provide a basis for validation of constitutive laws and the improvement of reduced-order models. Future work will also focus on stochastic characterization of terrain response and how underlying soil variability affects interfacial stresses modeling. In fact, even under laboratory controlled conditions, penetration plate tests have highlighted significant soil variability, warranting for statistical interpretation of experimental data.

REFERENCES

[1] Meirion-Griffith, G., and Spenko, M., "A modified pressure–sinkage model for small, rigid wheels on deformable terrains," Journal of Terramechanics, Volume 48, Issue 2, pp. 149-155, April, 2011.

[2] Wong, J.Y., "Data processing methodology in the characterization of the mechanical properties of terrain," Journal of Terramechanics, 17(1):13 – 41, 1980.

[3] Winter, A., "Biologically Inspired Mechanisms for Burrowing in Undersea Substrates," Ph.D. Thesis, Massachusetts Institute of Technology, 2010.

[4] Moreland, S., Skonieczny, K., Wettergreen, D., "Soil Motion Analysis System for Examining Wheel-Soil Shearing," 17th International Conference of the International Society for Terrain-Vehicle Systems, Virginia, USA, 2011.

[5] Iagnemma, K., A Laboratory Single Wheel Testbed for Studying Planetary Rover Wheel-Terrain Interaction, Technical Report 01-05-05, Field and Space Robotics Laboratory, Massachusetts Institute of Technology, Cambridge, MA, 2005.

[6] Beegle, L. W., Peters, G. H., Mungas, G. S., Bearman G. H., Smith, J. A., and Anderson, R. C., "Mojave Martian simulant: a new martian soil simulant," Lunar and planetary science, XXXVIII, 2007.

[7] Adrian, R. J., "Statistical Properties of Particle Image Velocimetry Measurements in Turbulent Flow, Laser Anemometry in Fluid Mechanics," Lisbon: Instituto Superior Tecnico, 1988, pp. 115–29.

[8] Keane, R. D., and Adrian, R.J., "Theory of Cross-Correlation Analysis of PIV Images," Applied Scientific Research, Vol. 49, Netherlands, 1992, pp.191-215.

[9] Adrian, R. J., "Twenty Years of Particle Image Velocimetry," Experiments in Fluids, Vol. 39, 2005, pp. 159–169.

[10] Sielamowicz, I., Błoński, S., and Kowalewski, T. A., "Digital Particle Image Velocimetry (DPIV) Technique in Measurements of Granular Material Flows," Chemical Engineering Science, Vol. 61, 2006, pp. 5307 – 5317.

[11] Jain, N., Ottino, J. M., and Lueptow R. M., "An Experimental Study of the Flowing Granular Layer in a Rotating Tumbler," Physics of Fluids, Vol. 14, 2002, pp. 572-582.

[12] Pudasaini, S. P., Hsiau, S. S., Wang, Y, and Hutter, K., "Velocity Measurements in Dry Granular Avalanches Using Particle Image Velocimetry - Technique and

Comparison with Theoretical Predictions," Physics of Fluids, Vol. 17, 2005.

[13] Barnett; C. M., Bengough, A. G., and McKenzie, B. M., "Quantitative Image Analysis of Earthworm-Mediated Soil Displacement," Biology and Fertility of Soils, 2009, Vol. 45, pp. 821-828.

[14] Saengprachatanarug, K., Ueno, M., Taira, E., and Okayasu, T., "Modeling of Soil Displacement and Soil Strain Distribution Calculation under the Traveling Wheel," 17th Int. ISTVS Conference, Blacksburg, Virginia, 2011.

[15] Wong, J. Y., "Behaviour of Soil beneath Rigid Wheels, Journal of agricultural Engineering," Vol. 12(4), 1967, pp. 257-269.

[16] Thielicke, W., and Stamhuis, E. J., "PIVlab – Time-Resolved Digital Particle Image Velocimetry Tool for Matlab," 2010.

[17] Adrian, R. J., and Westerweel, J., Particle Image Velocimetry, Cambridge University Press, New York, 2011.

[18] Keane, R. D., and Adrian, R. J., "Theory of Cross-Correlation Analysis of PIV Images," Applied Scientific Research, Vol. 49, Netherlands, 1992, pp.191-215.

[19] Wulfmeier, M., "Development of a Particle Image Velocimetry Method for Analysis of Mars Rover Wheel-Terrain Interaction Phenomena", B.S. Thesis, Gottfried Wilhelm Leibniz Universitaet Hannover, 2012.

[20] Nagatani, K., Ikeda, A., Sato, K., and Yoshida, K. "Accurate estimation of drawbar pull of wheeled mobile robots traversing sandy terrain using built-in force sensor array wheel," Proceedings of the International Conference on Robots and System, pp. 2373-2378, St. Louis, MO, October, 2009.

[21] Bekker, M. G., Theory of Land Locomotion, University of Michigan Press, Ann Arbor, MI, 1956.

[22] Reece, A. R., "Principles of soil-vehicle mechanics," Proc. Instn. Mech. Engrs., Vol. 80, Pt 2A No 2, 1965.

[23] Wong, J. Y., Theory of ground vehicles - 3rd ed., 528 p., New York, Wiley, 2001.

[24] Karafiath, L. L. and Nowatzki, E. A., Soil Mechanics for Off-Road Vehicle Engineering, Trans Tech Publications, Series on rock and soil mechanics Vol.2, No.5, Clausthal, West Germany, 1978.

[25] Onafeko, O., and Reece, A. R., "Soil Stresses and Deformations beneath Rigid Wheels," Journal of Terramechanics, Vol. 4(1), 1967.

[26] Wong, J. Y., and Reece, A. R., "Prediction of rigid wheel performance based on the analysis of soil-wheel stresses part I," Journal of Terramechanics, Vol. 4, No. 1, pp. 81-98, 1967.

[27] Wong, J. Y., and Reece, A. R., "Prediction of rigid wheel performance based on the analysis of soil-wheel stresses part II," Journal of Terramechanics, Vol. 4, No. 2, pp. 7-25, 1967.

[28] Janosi, Z., and Hanamoto, B., "Analytical determination of drawbar pull as a function of slip for tracked vehicles in deformable soils," 1st International Conference on Terrain-Vehicle Systems, Turin, Italy, 1967.

[29] Senatore, C., and Iagnemma, K., "Direct Shear Behavior of Dry, Granular Soils for Low Normal Stress with Application to Lightweight Robotic Vehicle Modelling," Proceedings of the International Symposium of the International Society of Terrain-Vehicle Systems, 2011.